RESEARCH ARTICLE | MAY 10 2023

Chimera states in multiplex networks: Chameleon-like across-layer synchronization

Special Collection: Chimera states: from theory and experiments to technology and living systems

Ralph G. Andrzejak ✉ ; Anaïs Espinoso

Chaos 33, 053112 (2023)
https://doi.org/10.1063/5.0146550

Chimera states in multiplex networks: Chameleon-like across-layer synchronization

Cite as: Chaos 33, 053112 (2023); doi: 10.1063/5.0146550
Submitted: 14 February 2023 · Accepted: 19 April 2023 ·
Published Online: 10 May 2023

Ralph G. Andrzejak[1,a)] and Anaïs Espinoso[1,2]

AFFILIATIONS

[1]Department of Information and Communication Technologies, Universitat Pompeu Fabra, Carrer Roc Boronat 138, 08018 Barcelona, Catalonia, Spain
[2]Institute for Bioengineering of Catalonia (IBEC), The Barcelona Institute of Science and Technology, Carrer Baldiri Reixac 10-12, 08028 Barcelona, Catalonia, Spain

Note: This paper is part of the Focus Issue on Chimera states from theory and experiments to technology and living systems.
[a)]**Author to whom correspondence should be addressed:** ralph.andrzejak@upf.edu

ABSTRACT

Different across-layer synchronization types of chimera states in multilayer networks have been discovered recently. We investigate possible relations between them, for example, if the onset of some synchronization type implies the onset of some other type. For this purpose, we use a two-layer network with multiplex inter-layer coupling. Each layer consists of a ring of non-locally coupled phase oscillators. While oscillators in each layer are identical, the layers are made non-identical by introducing mismatches in the oscillators' mean frequencies and phase lag parameters of the intra-layer coupling. We use different metrics to quantify the degree of various across-layer synchronization types. These include phase-locking between individual interacting oscillators, amplitude and phase synchronization between the order parameters of each layer, generalized synchronization between the driver and response layer, and the alignment of the incoherent oscillator groups' position on the two rings. For positive phase lag parameter mismatches, we get a cascaded onset of synchronization upon a gradual increase of the inter-layer coupling strength. For example, the two order parameters show phase synchronization before any of the interacting oscillator pairs does. For negative mismatches, most synchronization types have their onset in a narrow range of the coupling strength. Weaker couplings can destabilize chimera states in the response layer toward an almost fully coherent or fully incoherent motion. Finally, in the absence of a phase lag mismatch, sufficient coupling turns the response dynamics into a replica of the driver dynamics with the phases of all oscillators shifted by a constant lag.

Chimera states,[1–3] which are paradigmatic for the coexistence of synchronization and desynchronization, can be found even in very small, isolated networks.[4,5] Networks in nature, however, often consist of several interacting layers. In many cases, such as communicating brain areas, neither complete synchronization nor complete desynchronization would allow for a proper function. Instead, some partial synchronization is essential not only within layers but also across layers. Motivated by this bridge to real-world dynamics, recent work analyzed chimera states in multilayer networks, revealing different across-layer synchronization types, such as identical or almost identical,[6–11] generalized,[6] relay,[11–13] forced,[14,15] alignment,[6,14–19] frequency,[8] and phase synchronization.[20,21] Are there relations between these different synchronization types? Does some type generally imply some other type? Do they occur at the same coupling strengths? How do they depend on the heterogeneity of the network? To address these questions, we compose a whole battery of measures, each defined to detect one specific type of across-layer synchronization. We apply this battery of measures to a multiplex network with driver-response inter-layer coupling and a parameter mismatch between layers. In dependence on this mismatch and coupling strength, different compositions of synchronization arise. We here refer to this finding as chameleon-like across-layer synchronization and conclude that this versatility may contribute to the importance of synchronization in natural and human-made multilayer networks.

I. INTRODUCTION

The study of chimera states in multilayer networks showed from early on that couplings between network layers can induce or

destabilize chimera states in individual layers.[7–13,19,21–32] Apart from ring networks,[6–8,10–19,22–29] two-dimensional lattices[30–32] with a multiplex inter-layer coupling were analyzed. Further studies addressed the role of coupling delays,[12,22–25] inter-layer couplings with temporal fluctuations,[10,27] of limited duration,[26] and with nonlinear inertia,[9] as well as intra-layer coupling strengths adapting to the phase difference of interacting oscillators.[21,33] Chimera states were described in bipartite networks[34,35] and semirings with reflecting connectivity.[36] A further focus of attention is on across-layer control of chimera states.[6,12,16–18,27] Relay synchronization was demonstrated in triplex networks,[11–13] and forced synchronization was studied in networks of 20 layers.[14,15] Apart from identical or almost identical synchronization between all oscillator pairs,[6–11] two multiplexed rings can show alignment synchronization, for which the coherent domains attain the same[6,14–19] or antipodal[19] positions on the rings of both layers. Generalized synchronization[37–39] can be induced by a driver-response inter-layer coupling in multiplexed rings.[6] The layers' mean frequencies can be entrained, overcoming an across-layer mismatch in the oscillators' natural frequency.[8] Phase synchronization[40] between the order parameters of two rings each consisting of different numbers of oscillators and with an across-layer mismatch in the oscillators' natural frequencies was demonstrated in Ref. 20. In this non-multiplex setting, a bidirectional coupling from the order parameter phase of one layer to the individual oscillators of the other layer was used.[20] In multiplex networks, phase synchronization can be attained between individual oscillators.[21] We here return to the network architecture of Ref. 6 to investigate relations between some of these synchronization types. Our results show that this network exhibits a variety of across-layer synchronization types, which can coexist in different combinations. We introduce the term chameleon-like across-layer synchronization to refer to this changeableness of the system.

II. NETWORK DEFINITION

We study a network in which the first layer X drives the second layer Y via a unidirectional inter-layer multiplex coupling. Each layer consists of a ring of $N = 50$ identical phase oscillators connected via a non-local intra-layer coupling within a rectangular kernel of broadness $b = 18$. The phases of individual oscillators $\phi_{x,j}(t)$ in the driver X are not influenced by the inter-layer coupling but only by the intra-layer coupling. In contrast, the phase $\phi_{y,j}(t)$ of each individual oscillator j in the response Y is influenced by the intra-layer coupling and receives the inter-layer coupling with strength ε from oscillator j in X,

$$\dot{\phi}_{x,j}(t) = \nu_x - \frac{1}{2b}\sum_{k=j-b}^{j+b} \sin\left(\phi_{x,j}(t) - \phi_{x,k}(t) + \alpha_x\right), \tag{1}$$

$$\dot{\phi}_{y,j}(t) = \nu_y - \varepsilon \sin\left(\phi_{y,j}(t) - \phi_{x,j}(t)\right) - \frac{1}{2b}\sum_{k=j-b}^{j+b} \sin\left(\phi_{y,j}(t) - \phi_{y,k}(t) + \alpha_y\right) \tag{2}$$

for $j = 1, \ldots, N$. It is this ordered $j \to j$ inter-layer coupling that defines the multiplex architecture. The oscillators in the driver layer have the natural frequency ν_x and the phase lag parameter α_x. The parameters in the response ν_y and α_y are, in general, set differently from the corresponding values in the driver, and we denote the resulting mismatches between the layers by $\Delta\nu = \nu_y - \nu_x$ and $\Delta\alpha = \alpha_y - \alpha_x$. According to the layer's ring architecture, sums and differences of oscillator indices in Eqs. (1) and (2) are to be understood as modulo N. Starting from random initial conditions of the phases $\phi_{x,j}(t = 0)$ and $\phi_{y,j}(t = 0)$, which are independently and uniformly distributed in $(0, 2\pi]$, we integrate the dynamics using a fourth-order Runge–Kutta scheme with a sampling time of $\Delta t = 0.05$.

Like stated above, for the purpose of this study, we have to introduce a battery of measures each defined to assess a specific type of synchronization. This at first requires to extract a number of variables from the dynamics of individual layers. We here define them for the driver X, analogous definitions hold for the response Y. For each oscillator, the instantaneous frequency $\omega_{x,j}(t)$ is determined from the finite difference of the phase,

$$\omega_{x,j}(t) = \frac{\phi_{x,j}(t) - \phi_{x,j}(t + \Delta t)}{\Delta t}. \tag{3}$$

The network's mean-field is represented by the complex Kuramoto order parameter,[41]

$$Z_x(t) = \frac{1}{N}\sum_{j=1}^{N} e^{i\phi_{x,j}(t)} = R_x(t)e^{i\Phi_x(t)}, \tag{4}$$

with imaginary unit i, order parameter amplitude $R_x(t)$, and order parameter phase $\Phi_x(t)$.

Throughout this study, we set $\nu_x = 0$ and $\alpha_x = 1.485$. At these parameter values in combination with $N = 50$, $b = 18$, the driver layer spontaneously enters into a chimera state for the majority of random initial conditions. The chimeric segregation into two complementary groups can be appreciated in the spatiotemporal evolution of the oscillators' instantaneous frequencies $\omega_{x,j}(t)$ in Fig. 1(a). In a high-coherence group, all oscillators jointly rotate at an almost constant frequency $\omega_{x,j}(t)$. This frequency is negative; i.e., the rotation is clockwise. For the remaining oscillators, which form the low-coherence group, the frequencies $\omega_{x,j}(t)$ show an apparent irregular spatiotemporal profile. Hence, while all oscillators have the same equation of motion [Eq. (1)], this spatial symmetry of the network structure is broken by its dynamics.

Figure 1(a) furthermore shows that the positions of the high- and low-coherence group drift along the extension of the ring during the course of time.[42] To quantify the across-layer synchronization of this drifting motion, we at first determine the momentary position of the low-coherence group in Y. For this purpose, we use the temporal variability of frequencies, resulting in a spatial profile across $j = 1, \ldots, N$ for a certain time t,

$$\vartheta_{x,j}(t) = \sigma\left(\omega_{x,j}(t')\right)_{t' \in [t-T,t]}. \tag{5}$$

Here, $\sigma(\cdot)_{\_}$ denotes the standard deviation across the specified time interval sampled in steps of Δt. We use an interval of $T = 100$ time units, which is short compared to the time scale of the drifting motion but long enough to estimate the profile of $\vartheta_{x,j}(t)$. Since the oscillators of the low-coherence group show higher temporal variability in $\omega_{x,j}(t)$ as compared to the ones of the high-coherence

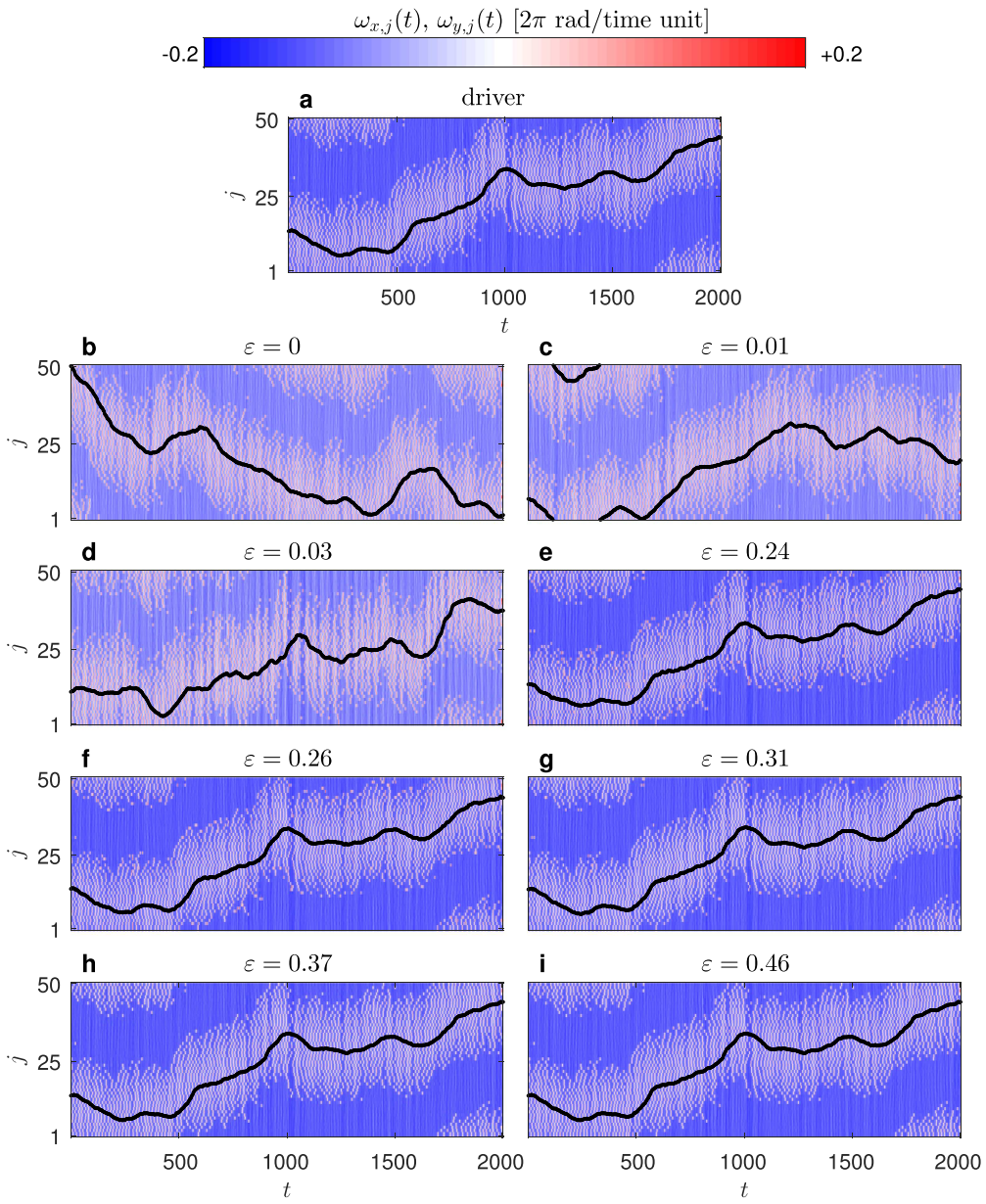

FIG. 1. Cascaded onset of synchronization. (a) Profiles of instantaneous frequencies $\omega_{x,j}(t)$ and the center of the low-coherence group $C_x(t)$ (black line) for the driver X. We display 2000 time units of the evaluation interval I, which spans 90 000 time units. The lag of $C_x(t)$ with regard to drift of the low-coherence group arises since $C_x(t)$ estimates the average position across the most recent $T = 100$ time units [Eqs. (5)–(7)]. For the illustration of this figure, $C_x(t)$ is calculated every one time unit, instead of only every $T = 100$ time units. (b)–(i) is the same as (a) but for the response: $\omega_{y,j}(t)$ and $C_y(t)$. Inter-layer coupling ε is indicated above each panel. Other parameters: $N = 50$, $b = 18$, $\nu_x = 0$, $\nu_y = 0.2$ (i.e., $\Delta\nu = 0.2$), $\alpha_x = 1.485$, $\alpha_y = 1.513$ (i.e., $\Delta\alpha = 0.028$). All panels have the same range of j and t.

group [see again Fig. 1(a)], the $\vartheta_{x,j}(t)$ profile shows a bump centered at indices j corresponding to the low-coherence group's position on the ring. We, therefore, interpret $\vartheta_{x,j}(t)$ as a circular distribution[43] and determine its circular mean direction. To link this direction to our network, we just have to map back and forth between the domain of the arg function of $(-\pi, \pi]$ and the extension of the ring $(0, N]$. Accordingly, for each oscillator with index j, a vector with length $\vartheta_{x,j}(t)$ and angle $\frac{2\pi j - \pi N}{N}$ is defined in the complex plane. The

angle of the resultant mean vector across all N oscillators,

$$\psi_x(t) = \arg\left[\frac{1}{N}\sum_{j=1}^{N}\vartheta_{x,j}(t)\cdot e^{i\frac{2\pi j-\pi N}{N}}\right], \tag{6}$$

can then be used to determine the center of the profile's bump,

$$C_x(t) = N\frac{\psi_x(t)+\pi}{2\pi}. \tag{7}$$

Therefore, $C_x(t)$ provides the center of the low-coherence group with values in $(0, N]$. The variables $\omega_{y,j}(t), R_y(t), \Phi_y(t)$, and $C_y(t)$ characterizing the response dynamics Y are defined analogously to the corresponding quantities in X.

To test for generalized synchronization between the driver and response, we use a replica of the response layer Y as auxiliary response layer Y'. This auxiliary response is obtained from a further realization of Eq. (2), starting from different random initial conditions but driven by the same $\phi_{x,j}(t)$ like the primary response Y. Like further described in Sec. III, this auxiliary response is used exclusively to test for generalized synchronization and no further variables are extracted from it. Technically, the driver X, response Y, and auxiliary response Y' jointly form $3 \cdot N$ coupled differential equations, which we integrated simultaneously using the aforementioned fourth-order Runge–Kutta scheme with $\Delta t = 0.05$ time units starting from $3 \cdot N$ independent random initial conditions.

During the first 1×10^3 time units, the inter-layer coupling was still kept off. Therefore, during this initial period, all three layers could settle to a chimera state, with Y and Y' not yet being influenced by X. For our finite-size ring networks, chimera states can suddenly collapse to a fully coherent state in which all phases become equal and the order parameter amplitude attains its maximal value of one.[44,45] Furthermore, after the initialization with random phases, the network can directly go to this fully coherent state without ever forming a chimera state. If any of the three layers went to a fully coherent state during the initial 1×10^3 time units, the realization was discarded and the dynamics was started again with a set of new random initial conditions. Provided that all layers entered into chimera states, the inter-layer coupling with strength ε was turned on at 1×10^3 time units. The dynamics was then evaluated during the interval $I = [1 \times 10^4, 1 \times 10^5]$ time units. In this way, transients caused by the coupling onset could fade out between 1×10^3 and 1×10^4 time units. In case the driver layer collapsed after the initial 1×10^3 time units but before the end of the simulation at 1×10^5 time units, the realization was also discarded and the simulation was started over. As we describe below, the driving can cause a degeneration of the chimera state in response to an almost fully coherent or almost fully incoherent state. This reflects, however, an effect of the coupling instead of the transient nature of chimera states. Therefore, no reinitialization of the simulation was done if the chimera state degenerated in the response or the auxiliary response after the coupling onset at $1 \cdot 10^3$ time units.

III. SYNCHRONIZATION MEASURES

Since the aim of our study is to characterize different types of synchronization between the driver layer X and response layer Y, we have to use a battery of measures, each defined to detect one specific type of across-layer synchronization. For this purpose, we combine some methods devised in our earlier work[6,20] with additional *ad hoc* measures. Synchronization between the mean-fields is assessed separately for the amplitudes and phases of the order parameters $Z_x(t)$ and $Z_y(t)$. We denote the Pearson correlation coefficient between the amplitudes $R_x(t)$ and $R_y(t)$ across $t \in I$ by K. For independent layers, K values close to zero are expected. The range of $0.99 \leq K < 1$ is used to detect *non-identical order parameter amplitude synchronization*. The lower threshold of 0.99 is high but otherwise arbitrary. The upper limit of $K = 1$ indicates a perfect correlation throughout the evaluation interval I. In this case, it remains to be ruled out that $R_x(t)$ and $R_y(t)$ have a constant offset between them before concluding to *identical order parameter amplitude synchronization*.

To quantify the dependence between the order parameter phases $\Phi_x(t)$ and $\Phi_y(t)$, we at first unwrap them from the circular domain to the infinite domain. We then determine their instantaneous difference,

$$\Delta\Phi(t) = \Phi_x(t) - \Phi_y(t), \tag{8}$$

and therefrom the accumulated order parameter phase difference,[20]

$$S = \frac{\max\{\Delta\Phi(t)\}_{t\in I} - \min\{\Delta\Phi(t)\}_{t\in I}}{2\pi}, \tag{9}$$

where $\{\cdot\}_{\_}$ indicates that the extrema are determined across the specified time interval sampled in steps of Δt. If $\Phi_x(t)$ and $\Phi_y(t)$ rotate with a constant phase lag throughout the evaluation interval I, we get $\max\{\Delta\Phi(t)\}_{t\in I} = \min\{\Delta\Phi(t)\}_{t\in I}$ and obtain the minimal value of $S = 0$. This represents *order parameter phase synchronization with strong phase-locking*. Note that for this condition to be fulfilled, the phase difference has to be constant but does not have to be zero: $\Delta\Phi(t) = \text{const} \geq 0$. In contrast, any temporal variability of $\Delta\Phi(t)$ leads to $S > 0$. However, as long as the order parameters do not lap each other in the complex plane, the value of S remains below 1. Accordingly, $0 < S < 1$ corresponds to *order parameter phase synchronization with weak phase-locking*. As soon as one order parameter completes one more rotation than the other order parameter, $\Delta\Phi(t)$ grows by 2π, and S increments by 1. Hence, $S \geq 1$ indicates that the order parameter phases are not locked and the order parameters of the driver and response are not phase synchronized. Provided that we detect strong or weak phase-locking, we determine the average order parameter phase lag,

$$\overline{\Delta\Phi} = \langle\Delta\Phi(t)\rangle_{t\in I}, \tag{10}$$

where $\langle\cdot\rangle_{\_}$ indicates that the average is taken across the specified time interval sampled in steps of Δt. For strong phase-locking, averaging would not be needed because the phase lag $\Delta\Phi(t)$ is constant, but Eq. (10) remains applicable.

Apart from the macroscopic quantity S, we determine the accumulated phase differences s_j for pairs of individual oscillators across $j = 1, \ldots, N$. The s_j are determined in the same way as S, but using the phase differences of individual oscillators $\Delta\phi_j(t) = \phi_{x,j}(t) - \phi_{y,j}(t)$ instead of the order parameter phase difference $\Delta\Phi(t)$. The fraction of weakly phase-locked oscillator pairs is then given by

$$L_w = \frac{\#\{j|0 < s_j < 1 \wedge j = 1, \ldots, N\}}{N}, \tag{11}$$

with # denoting cardinality (see Refs. 8, 21, 30, and 32 for similar approaches). Analogously, the fraction of strongly phase-locked oscillator pairs is

$$L_s = \frac{\#\{j|s_j = 0 \wedge j = 1,\ldots,N\}}{N}. \tag{12}$$

We use the range of $0.5 \leq L_w < 1$ to conclude *partial oscillator pair phase synchronization with weak phase-locking*, and $L_w = 1$ implies *complete oscillator pair phase synchronization with weak phase-locking*. The same thresholds are applied to L_s to assess *partial or complete oscillator pair phase synchronization with strong phase-locking*.

To quantify the degree to which the drifting motion of the low-coherence group in the driver X influences the one in the response Y, we use the normalized distance between the groups' positions,

$$\Delta C(t) = \frac{\min\{|C_x(t) - C_y(t)|, N - |C_x(t) - C_y(t)|\}}{\frac{N}{4}}. \tag{13}$$

Here, $|\cdot|$ denotes the absolute value, and the min-operation ensures that the shorter of the two distances on the ring is used. The nominator of Eq. (13) takes its minimum of 0 if $C_x(t) = C_y(t)$. Its maximum of $\frac{N}{2}$ is obtained if $C_x(t)$ and $C_y(t)$ are in antipodal positions. A nominator of $\frac{N}{4}$ is expected for independent dynamics. Accordingly, due to the denominator of Eq. (13), $\Delta C(t)$ is in units of this expected value for independent dynamics. The average chimera group distance is determined from

$$\overline{\Delta C} = \langle \Delta C(t) \rangle_{t\in I}. \tag{14}$$

Only in the case of this temporal average taken in Eq. (14), t is incremented in steps of T instead of the sampling time Δt [see again Eq. (5)]. For independent dynamics, we expect $\overline{\Delta C} = 1$. The maximal value of $\overline{\Delta C} = 2$ is obtained if a low-coherence group in the response is always antipodal to the one in the driver. We use a range of $0 < \overline{\Delta C} \leq 0.05$ to conclude *non-identical group alignment synchronization*. If the drifting motion of the low-coherence group in the response is identical to the one in the driver, we get $\overline{\Delta C} = 0$ and *identical group alignment synchronization*.

The approach to determine the average chimera group distance via Eqs. (5)–(7) is based on the assumption that the $\vartheta_{x,j}(t)$ and $\vartheta_{y,j}(t)$ profiles actually have a bump. To check the validity of this assumption for the driver, we determine the profile's spatial coefficient of variation,

$$\xi_x(t) = \frac{\sigma\{\vartheta_{x,j}(t)\}_{j=1,\ldots,N}}{\mu\{\vartheta_{x,j}(t)\}_{j=1,\ldots,N}}, \tag{15}$$

where $\sigma\{\cdot\}_{\_}$ and $\mu\{\cdot\}_{\_}$ denote standard deviation and mean, respectively, across the given indices. The average across the evaluation interval is

$$\overline{\xi_x} = \langle \xi_x(t) \rangle_{t\in I}. \tag{16}$$

For the response Y, the quantity $\overline{\xi_y}$ is calculated analogously. The driver X, which has fixed parameters and is not influenced by the coupling, always shows chimera states and high values of $\overline{\xi_x} \approx 0.55$. For the response Y, the quantity $\overline{\xi_y}$ depends on the parameter mismatch and inter-layer coupling strength. We found by visual inspection of the dynamics that for values $\overline{\xi_y}$ lower than approximately 0.30, a clear delineation of the response's low- and high-coherence group was not given. In this case, the average chimera group distance $\overline{\Delta C}$ cannot be well-defined.

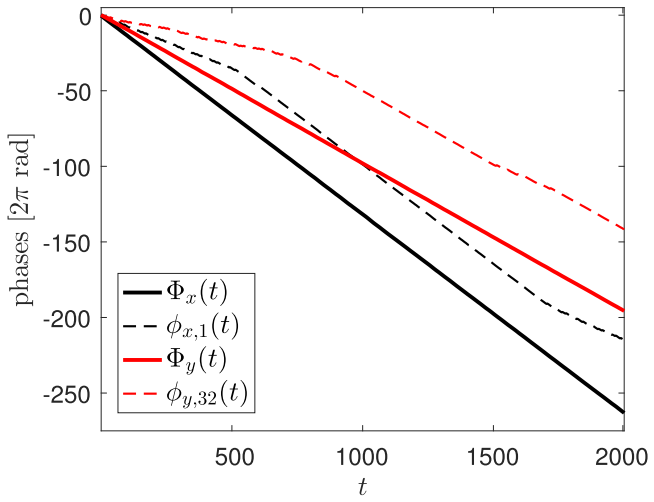

FIG. 2. While in the high-coherence group, individual oscillators are locked to the mean-field. Black: the order parameter phase of the driver $\Phi_x(t)$ and the phase of an exemplary individual oscillator $\phi_{x,j=1}(t)$ for the realization shown in Fig. 1(a). Red: Same as black but for the realization of the response shown in Fig. 1(b) and using oscillator $j = 32$ as an example. All parameters are the same as in Fig. 1: $N = 50$, $b = 18$, $\nu_x = 0$, $\nu_y = 0.2$ (i.e., $\Delta\nu = 0.2$), $\alpha_x = 1.485$, $\alpha_y = 1.513$ (i.e., $\Delta\alpha = 0.028$).

The so-called auxiliary system approach[38,39] detects *generalized synchronization*[37–39] between the driver X and response Y from identical synchronization between the response Y and the auxiliary response Y'. We quantify the difference between Y and Y' by

$$\delta(t) = \frac{1}{N}\sum_{j=1}^{N}\left|\sin\left(\frac{\phi_{y,j}(t) - \phi_{y',j}(t)}{2}\right)\right|. \tag{17}$$

This metrics was introduced in Ref. 6 and adapted in Ref. 21. If during the evaluation interval we find $\delta(t) = 0$, this indicates identical synchronization between Y and Y' and, therefore, generalized synchronization between X and Y[46] (see also Refs. 47 and 48). To express the two possible outcomes, we define the measure $G = 1$ if there is generalized synchronization and $G = 0$ otherwise.

IV. RESULTS

In the first part of this section, we provide detailed results for single realizations of exemplary dynamics (Fig. 1). A particular emphasis is given to group alignment synchronization (Fig. 1) as well as to the evolution of phases and phase differences of individual oscillators and order parameters (Figs. 2 and 3). Evaluating all synchronization measures at the collective level (Table I), we show that these exemplary dynamics represent different combinations of across-layer synchronization types.

Figure 1 shows profiles of the instantaneous phase velocities for the driver $\omega_{x,j}(t)$ and response $\omega_{y,j}(t)$ in dependence on time

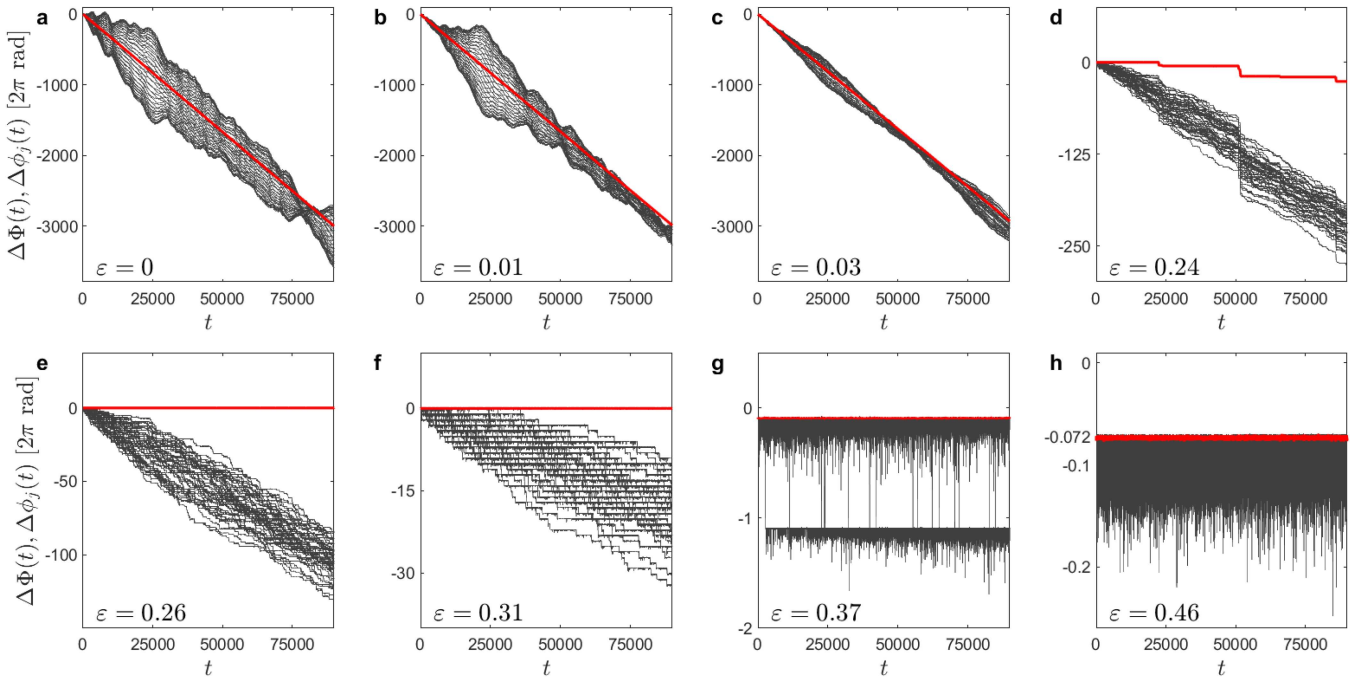

FIG. 3. Order parameters phase-lock before individual oscillators do. Instantaneous phase differences of order parameters (red) and individual oscillator pairs (gray) in dependence on time and for exemplary inter-layer coupling strengths. Results shown in panels (a)–(h) are, respectively, for the realizations shown in Figs. 1(b)–1(i), but here covering the entire evaluation interval. Note the different ordinate scalings across panels. In panel (h), an extra label to the y axes is placed at −0.072. This corresponds to −26°, which is the average order parameter phase lag $\overline{\Delta\Phi}$ around which $\Delta\Phi(t)$ fluctuates for this ε (see Table I). All parameters are the same as in Fig. 1: $N = 50$, $b = 18$, $\nu_x = 0$, $\nu_y = 0.2$ (i.e., $\Delta\nu = 0.2$), $\alpha_x = 1.485$, $\alpha_y = 1.513$ (i.e., $\Delta\alpha = 0.028$).

t and the oscillator index j. Results are shown for fixed $\Delta\nu = 0.2$ and $\Delta\alpha = 0.028$ and eight selected values of the inter-layer coupling strength ε. In general, we use new random initial conditions for each realization. However, the same set of $3 \cdot N$ independent random initial conditions is used across all simulations of Fig. 1. This allows us to show the profile of the driver X only once since it is fully determined by its N initial conditions [Fig. 1(a)]. Moreover, changes observed in the profiles of the response Y [Figs. 1(b)–1(i)]

TABLE I. Results for the examples displayed in Fig. 1 and further analyzed in Fig. 3, with the corresponding panels indicated in the first two columns. The inter-layer coupling ε is given in the third column. Recall that Fig. 1(a) displays the driver dynamics, which does not depend on the coupling and is common to the response dynamics in Figs. 1(b)–1(i). Results in this table are obtained from the entire evaluation interval of 90 000 time units, while Fig. 1 shows only an exemplary window of 2 000 time units. Boldface values indicate synchronization assessed by the respective measure as detailed in the following: $0 < \overline{\Delta C} \leq 0.05$, non-identical group alignment synchronization; $0 < S < 1$, order parameter phase synchronization with weak phase-locking; $G = 1$, generalized synchronization; $0.5 \leq L_w < 1$, partial oscillator pair phase synchronization with weak phase-locking and $L_w = 1$, complete oscillator pair phase synchronization with weak phase-locking; and $0.99 \leq K < 1$, non-identical order parameter amplitude synchronization. Other forms and/or stronger degrees of synchronization are not detected for the examples included here. In particular, there is no oscillator pair phase synchronization with strong phase-locking; hence, $L_s = 0$. Recall that the average order parameter phase difference $\overline{\Delta\Phi}$ is not determined (n.d.) in the absence of order parameter phase-locking as detected by $S > 1$. All parameters are the same as in Fig. 1: $N = 50$, $b = 18$, $\nu_x = 0$, $\nu_y = 0.2$ (i.e., $\Delta\nu = 0.2$), $\alpha_x = 1.485$, $\alpha_y = 1.513$ (i.e., $\Delta\alpha = 0.028$).

Figure 1	Figure 3	ε	$\overline{\Delta C}$	S	G	L_w	K	L_s	$\overline{\Delta\Phi}$
(b)	(a)	0	1.0	2997	0	0	0.000 87	0	n.d.
(c)	(b)	0.01	0.91	2989	0	0	−0.0061	0	n.d.
(d)	(c)	0.03	0.42	2929	0	0	0.028	0	n.d.
(e)	(d)	0.24	**0.044**	26.13	0	0	0.62	0	n.d.
(f)	(e)	0.26	**0.024**	**0.79**	0	0	0.79	0	−51°
(g)	(f)	0.31	**0.010**	**0.38**	**1**	0	0.91	0	−42°
(h)	(g)	0.37	**0.0021**	**0.018**	**1**	**0.68**	0.98	0	−33°
(i)	(h)	0.46	**0.000 98**	**0.0077**	**1**	**1**	**0.99**	0	−26°

exclusively reflect the impact of the different coupling strengths ε from X to Y obtained for this set of N initial conditions used for Y. The auxiliary response Y' also has its own N initial conditions. It is not displayed in Fig. 1 because it is exclusively used to test for generalized synchronization.

The driver shows a chimera state with the characteristic segregation into a low- and high-coherence group and the drifting boundaries between these groups[42] [Fig. 1(a)]. Regarding the order parameter phase $\Phi_x(t)$ and the phase of exemplary individual oscillators $\phi_{x,1}(t)$, we first notice that they grow toward $-\infty$ (Fig. 2), which reflects that their clockwise rotation has, by convention, a negative phase velocity [see again Fig. 1(a)]. At the resolution of Fig. 2, the order parameter phase seems to grow linearly. However, small fluctuations can be detected when looking at its derivative, i.e., the instantaneous order parameter phase velocity (not shown). Phases of individual oscillators evolve less regularly. Looking back and forth between Figs. 1(a) and 2, one can verify that once oscillator $j = 1$ joins the high-coherence group, the momentary slope of $\phi_{x,1}(t)$ is on average the same as the one of $\Phi_x(t)$. This illustrates that high-coherence group oscillators are locked to the mean-field. Once the drifting of the groups causes the oscillator to switch back from the high-coherence to the low-coherence group, its phase loses grip and it is often lapped by the mean-field phase. In consequence, once the first oscillator turned again into a low-coherence group member, the absolute value of the slope of its phase $\phi_{x,1}(t)$ is again lower than the one of $\Phi_x(t)$.

For $\varepsilon = 0$, i.e., in the absence of an inter-layer coupling, the response shows a chimera state, which is independent from the one of the driver [Fig. 1(b)]. Due to the parameter mismatch $\Delta\nu = 0.2$ and $\Delta\alpha = 0.028$, the appearance of the Y dynamics is somewhat different from the one of X. It has less sharp boundaries between its high- and low-coherence group, and the drifting motion seems more erratic. Furthermore, the average absolute values of $\omega_{y,j}(t)$ are smaller than the ones of $\omega_{x,j}(t)$. As a consequence, the order parameter of the response rotates slower than the one of the driver. Therefore, the $\Phi_y(t)$ curve has a less negative slope than the one of $\Phi_x(t)$ in Fig. 2. Due to the lack of coupling between layers, the positions of the low-coherence groups for the driver $C_x(t)$ and response $C_y(t)$ evolve in an unrelated manner. When averaged across the entire evaluation interval, we, therefore, get a $\overline{\Delta C}$ value, which is consistent with the value of one expected for such independent dynamics (Table I). For $\varepsilon = 0.01$, the overall appearance of the response dynamics remains similar to the uncoupled case but with a different time course for the low-coherence group position $C_y(t)$. Indeed, $\overline{\Delta C}$ already drops below the aforementioned expected value [Fig. 1(c), Table I]. At $\varepsilon = 0.03$, one can notice a pronounced ripple pattern in the response dynamics, and the overall appearance of $\omega_{y,j}(t)$ seems to become even more erratic than for $\varepsilon = 0$ and $\varepsilon = 0.01$ [Fig. 1(d) vs Figs. 1(b) and 1(c)]. On the other hand, the drifting motion of the boundaries between the high- and low-coherence group in the response Y increasingly resembles the one of the driver X, resulting in a substantial decrease of $\overline{\Delta C}$ [Fig. 1(d), Table I].

At an inter-layer coupling of $\varepsilon = 0.24$, the average chimera group distance $\overline{\Delta C}$ has crossed the threshold used to detect non-identical group alignment synchronization [Fig. 1(e), Table I]. Upon further increase of the coupling, $\overline{\Delta C}$ diminishes further. However, it remains non-zero so that we do not get identical group alignment synchronization for the examples included in Fig. 1. Moreover, from around $\varepsilon \geq 0.24$, the response frequency profiles $\omega_{y,j}(t)$ increasingly resemble the one of the driver $\omega_{x,j}(t)$ [Fig. 1(a) vs Figs. 1(e)–1(i)]. As a consequence, the response frequency profiles $\omega_{y,j}(t)$ for different strong couplings also increasingly resemble each other. Therefore, while visual inspection of the response dynamics is helpful for comparing uncoupled and different weakly coupled dynamics, it fails to tell apart different strongly coupled dynamics. That is why we need the set of metrics introduced in Sec. III. They allow us to reveal changes in both the degree and form of across-layer synchronization across the entire range of inter-layer coupling strengths.

After focusing on group alignment synchronization (Fig. 1) and the evolution of phases (Fig. 2), we now proceed to inspect across-layer phase differences of individual oscillators and order parameters. Figure 3 shows differences between the unwrapped individual phases $\Delta\phi_j(t)$ and between the order parameter phases $\Delta\Phi(t)$ that underly the measures s_j and S, respectively. We first consider the case of zero inter-layer coupling [Fig. 3(a)]. Since both networks rotate clockwise and X rotates faster than Y, the difference of their mean-fields $\Delta\Phi(t) = \Phi_x(t) - \Phi_y(t)$ growths unboundedly into the negative domain, and we get $S \gg 1$ for the accumulated order parameter phase difference (Table I). In contrast to $\Delta\Phi(t)$, differences between individual phases $\Delta\phi_j(t)$ do not evolve monotonically. We already saw in Fig. 2 that oscillators in the low-coherence group rotate slower than the ones in the high-coherence group.[49] Therefore, despite that X is overall faster than Y, oscillators in the low-coherence group of X can still rotate slower than oscillators in the high-coherence group of Y. Therefore, while a certain oscillator j of X is in the low-coherence group and the multiplexed oscillator j of Y is in the high-coherence group, the curve $\Delta\phi_j(t) = \phi_{x,j}(t) - \phi_{y,j}(t)$ can have a positive slope. The largest negative slope of $\Delta\phi_j(t)$, in contrast, is obtained, while the oscillator with index j of X belongs to the high-coherence group and the one of Y to the low-coherence group. Intermediate slopes are obtained as long as both oscillators belong to the same group in their respective network. Since at $\varepsilon = 0$, the oscillators switch between the high- and low-coherence groups independently for X and Y, the slopes of the N curves of $\Delta\phi_j(t)$ change irregularly. There cannot be any phase-locking between individual oscillator pairs; hence, we get $s_j \gg 1$ for all j, and therefrom, $L_w = L_s = 0$ [Fig. 3(a), Table I]. A similar picture is obtained for $\varepsilon = 0.01$, notwithstanding that already a slight decrease of S can be noted [Fig. 3(b), Table I]. This decrease continues for $\varepsilon = 0.03$, and the $\Delta\phi_j(t)$ curves fan out less [Fig. 3(c), Table I]. This can be understood by connecting results from different synchronization measures. Recall that at this coupling, already, a stronger alignment of the centers of the low-coherence groups of X and Y across time is obtained [see again Fig. 1(d) and $\overline{\Delta C}$ in Table I]. As a consequence, pairs of oscillators with the same index j more often belong either both to the high-coherence group or both to the low-coherence group in X and Y.

A qualitatively different scenario is obtained for $\varepsilon = 0.24$ [Fig. 3(d)]. The $\Delta\Phi(t)$ curve shows a stick-jump behavior. During some time, it fluctuates around a non-zero value. Then, at some apparently random moment in time, this sticking behavior is interrupted by a jump. The order parameter of the driver suddenly laps the one of the response one or a few times, decreasing $\Delta\Phi(t)$ by 2π times the number of extra rotations. This jump is followed by a new

sticking period and so on. As a result of the sticking, S decreases substantially. As a result of the jumps, it remains clearly above one (Table I). A stick-jump behavior is also found for the phase differences of individual oscillator pairs $\Delta\phi_j(t)$. It can be observed that collective jumps of all oscillators coincide with particularly pronounced jumps in the order parameter [see again Fig. 3(d)]. Since jumps are found for all pairs of oscillators, not a single pair shows weak or even strong phase-locking. Hence, all s_j remain above one, and we continue to get $L_w = L_s = 0$ (Table I). The next transition is found for $\varepsilon = 0.26$ [Fig. 3(e)]. The difference of the order parameter phases $\Delta\Phi(t)$ does no longer grow toward $-\infty$, but instead fluctuates around a stable non-zero mean value. We, therefore, get $0 < S < 1$, indicating order parameter phase synchronization with weak phase-locking. Accordingly, we can now also determine the average phase lag $\overline{\Delta\Phi}$ (Table I). In contrast, all individual oscillator pairs continue to show a stick-jump behavior. The difference is that the average duration of the intervals during which the $\Delta\phi_j(t)$ curves stick gets longer such that the total growth of these curves is reduced. This reduction is further intensified at $\varepsilon = 0.31$ [Fig. 3(f)].

At $\varepsilon = 0.37$, for more than one half of the oscillator pairs, their curve $\Delta\phi_j(t)$ sticks during the entire evaluation interval, resulting in $L_w > 0.5$ [Fig. 3(g), Table I]. This means that we detect partial oscillator pair phase synchronization with weak phase-locking ($0.5 \leq L_w < 1$). For the remaining pairs, the driver oscillator laps its response oscillator once, resulting in $\Delta\phi_j(t) < -1$. This means that these oscillator pairs are not phase-locked. This example illustrates that for such stick-jump behavior, the assessment of weak phase-locking and, thereby, the value of L_w depends on the duration of the evaluation interval. For shorter and longer evaluation intervals, respectively, all N or not a single oscillator pair would be assumed to be weakly phase-locked. It is just a matter of whether the evaluation interval is long enough to capture their sporadic jumps. However, what does not depend on the observation time is the finding of $L_s = 0$ because not a single oscillator pair shows a constant phase lag, which would imply strong phase-locking. Finally, at $\varepsilon = 0.46$, for all oscillator pairs, the sticking outlasts the evaluation interval, resulting in $L_w = 1$. This indicates complete oscillator pair phase synchronization with weak phase-locking [Fig. 3(h), Table I]. Accordingly, at this coupling, not only the mean-field, as assessed by the order parameter, but also all individual oscillators of the response Y show weak phase-locking to their counterparts in the driver X. The absolute average phase lag between the order parameters $\overline{\Delta\Phi}$ decreases with the inter-layer coupling but remains non-zero (Fig. 3(h), Table I). A non-zero average phase lag is found also for the individual oscillators. In both cases, the phase lag is not constant, ruling out strong phase-locking. This is reflected in $S > 0$ and $s_j > 0$ for all j and, therefore, $L_s = 0$, throughout the examples included in Fig. 3.

How do the amplitudes of the order parameter behave upon the locking of the order parameter phases? Is there a relation between the order parameter amplitude correlation K and the accumulated order parameter phase difference S? For pairs of low-dimensional coupled chaotic dynamics, phase synchronization is conventionally defined by the weak phase-locking criterion.[40] For this criterion, the amplitudes of the individual dynamics are not taken into account. In particular, the amplitudes may remain uncorrelated between the two dynamics. For our two-layer network, the Pearson correlation coefficient K between the order parameter amplitudes $R_x(t)$ and $R_y(t)$ increases significantly once the order parameter phases start to lock (Table I), and this correlation is strengthened upon a further increase of the inter-layer coupling strength. Non-identical order parameter amplitude synchronization is reached at $\varepsilon = 0.46$. This is consistent with the aforementioned observation that at higher couplings, the response frequency profiles $\omega_{y,j}(t)$ increasingly resemble the one of the driver $\omega_{x,j}(t)$ [compare again Fig. 1(a) vs Figs. 1(e)–1(i)]. However, due to the parameter mismatches $\Delta\nu$ and $\Delta\alpha$, the network layers cannot synchronize identically. As a consequence, the correlation K remains below one, and we do not reach identical order parameter amplitude synchronization (Table I).

While identical synchronization is not possible between non-identical layers, we can get generalized synchronization between them.[6] Using the auxiliary system approach, we find this transition in between the examples shown Fig. 1(f) and 1(g). For $\varepsilon = 0.26$, there is no generalized synchronization ($G = 0$) between the driver and response, but at $\varepsilon = 0.31$, there is ($G = 1$). This implies that while the profiles displayed in Figs. 1(b)–1(f) still depend on the initial conditions of the response Y, the ones in Figs. 1(g)–1(i) are uniquely determined by the state of the driver shown in Fig. 1(a). In other words, there exists some function F such that $\omega_{y,j}(t) = F(\omega_{x,j}(t))$. As concluded in the previous paragraph, this function F cannot be simply the identity. Furthermore, note that at $\varepsilon = 0.31$, despite that the overall system shows generalized synchronization, none of the individual oscillator pairs is phase-locked. At $\varepsilon = 0.46$, both the order parameters and all oscillator pairs show phase synchronization, however, only with weak phase-locking. This means that the phase differences of the pair of order parameters and all pairs of individual oscillators are not constant [see again Fig. 3(h)]. Therefore, the function F relating the response Y to the driver X is not simply the phase lag operation. Accordingly, combining the results from G, K, S, and s_j, we can conclude that the system exhibits generalized synchronization with a non-trivial function F.

The results reviewed so far show how the synchronization measures allow detecting different types of across-layer synchronization. However, this part of the analysis was restricted to some exemplary inter-layer coupling strengths ε and fixed $\Delta\alpha = \alpha_y - \alpha_x$ and $\Delta\nu = \nu_y - \nu_x$. We now proceed by looking at results in the plane spanned by $\Delta\alpha$ and ε, keeping only $\Delta\nu = 0.2$ fixed (Fig. 4). Recall that these parameters only affect the response layer Y. The driver layer X has fixed α_x and ν_x and is not influenced by the unidirectional inter-layer coupling from X to Y. For the measures of synchronization $\overline{\Delta C}, S, L_w, L_s$, and K, we use a hot and cold color map for unsynchronized and synchronized dynamics, respectively. In this way, the transition from white to blue marks the onset of synchronization as assessed by the particular measure. Magenta indicates the strongest degree of synchronization for each measure. For the binary measure G, magenta indicates generalized synchronization, and black shows the absence thereof. For the spatial coefficient of variation $\overline{\xi_y}$ and the average order parameter phase lag $\overline{\Delta\Phi}$, a gray color map is used. The parameter range for which $\overline{\Delta\Phi}$ is not determined due to the lack of phase-locking is painted in red.

Results for the group alignment synchronization as assessed by the average chimera group distance $\overline{\Delta C}$ are shown in Fig. 4(a). For $\varepsilon = 0$, this distance is close to the expected value for such uncoupled layers: $\overline{\Delta C} \approx 1$. A first drop of $\overline{\Delta C}$ throughout the range

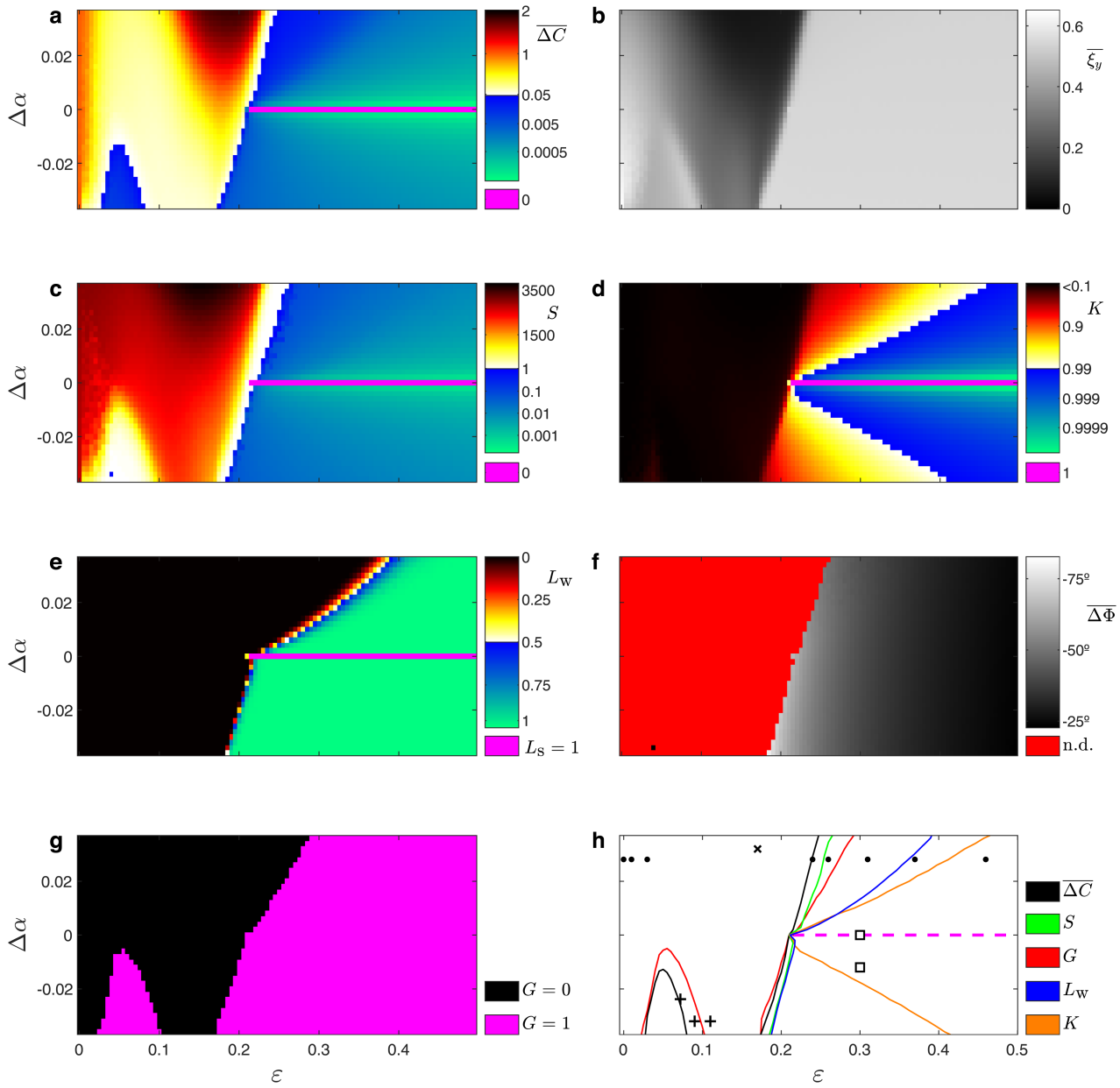

FIG. 4. Chameleon-like across-layer synchronization: In dependence on $\Delta\alpha$ and ε, different compositions of synchronization arise. Averages across 40 realizations. Panels (a) and (c)–(e): Hot colors, cold colors, and magenta indicate, respectively, no sync, sync, and the strongest degree of sync according to the corresponding measure. Log-scale for hot and cold colors in (d) and (a) and (c) only for cold colors. (a) Average chimera group distance. $\overline{\Delta C} > 0.05$: No sync. $0 < \overline{\Delta C} \leq 0.05$: Non-identical group alignment sync. $\overline{\Delta C} = 0$: Identical group alignment sync. (b) Spatial coefficient of variation in response's frequency profile $\overline{\xi_y}$. (c) Accumulated order parameter phase difference. $S \geq 1$: No sync. $0 < S < 1$: Order parameter phase sync, weak phase-locking. $S = 0$: Order parameter phase sync, strong phase-locking. (d) Order parameter amplitude correlation. $K < 0.99$: No sync. $0.99 \leq K < 1$: Non-identical order parameter amplitude sync. $K = 1$: Identical order parameter amplitude sync. (e) Fractions of weakly or strongly phase-locked individual oscillator pairs. $0 < L_w < 0.5, L_s = 0$: No sync. $0.5 \leq L_w < 1, L_s = 0$: Partial oscillator pair phase sync, weak phase-locking. $L_w = 1, L_s = 0$: Complete oscillator pair phase sync, weak phase-locking. $L_w = 0, L_s = 1$: Complete oscillator pair phase sync, strong phase-locking. (f) Average order parameter phase difference $\overline{\Delta\Phi}$. Red: not defined (n.d.) due to lack of phase-locking. (g) $G = 1$: Generalized sync. $G = 0$: No sync. (h) Lines indicating sync onset as assessed by each measure. Dashed magenta line: Range where response is replica of driver with phases of all oscillators shifted by a constant lag. Black dots, from left to right: parameters used in Figs. 1(b)–1(i); ×: Fig. 5(b); +, from left to right: Figs. 5(c)–5(e). White squares, top to bottom: Figs. 5(f)–5(g). All other parameters are the same as in Fig. 1.

of $\Delta\alpha$ is visible already for small inter-layer couplings ε. On the left of Fig. 4(a), two prominent tongues are found. A dark tongue is located at positive $\Delta\alpha$ around $\varepsilon \approx 0.18$. Here, the measure $\overline{\Delta C}$ has values of up to almost two. Recall that $\overline{\Delta C}$ is normalized by the value expected for independent layers $\left(\frac{N}{4}\right)$. Accordingly, a value of almost two means that the low-coherence groups in the driver and response are in almost antipodal positions on the ring $\left(\frac{N}{2}\right)$. However, for the parameters corresponding to this dark tongue constituted by high $\overline{\Delta C}$ values [Fig. 4(a)], very low values of $\overline{\xi_y}$ are found [Fig. 4(b)]. The low $\overline{\xi_y}$ values indicate that in this parameter range, the response does not show a clear segregation between the high- and low-coherence group. A look at some exemplary dynamics with parameters from the center of the dark tongue confirms that, in contrast to the driver X [Fig. 5(a)], the response Y [Fig. 5(b)] shows no chimera state. As a consequence, the position of the low-coherence group and, therefore, $\overline{\Delta C}$ is indeed not well-defined, as already suggested by low values of $\overline{\xi_y}$ [Fig. 4(b)].

For negative $\Delta\alpha$, a blue tongue of non-identical group alignment synchronization is found [Fig. 4(a)]. However, looking at the response for parameters close to this blue tongue, we find a further type of non-chimera dynamics [Figs. 5(c)–5(e)]. The Y layer switches intermittently between partly synchronized states and almost fully synchronized states. The partly synchronized states in the response appear as vertical stripes in which a low-coherent group seems to form at the position of the low-coherence group of the driver dynamics [Figs. 5(c)–5(e) vs Fig. 5(a)]. However, this formation disintegrates, and the response dynamics seems to go toward a fully synchronized state. Since each oscillator receives a different input via the multiplex coupling from X, however, a fully synchronized state cannot be reached. In particular, the oscillators in Y coupled to oscillators belonging to the low-coherence group in X deviate from the overall almost synchronized motion. The degree of incoherence in Y is small, but the group of affected oscillators is aligned to the low-coherence group in X. In consequence, during both the partly synchronized states and almost fully synchronized states, the response Y has a well-defined low-coherence group, which is aligned to the one in the driver X, resulting in low values of $\overline{\Delta C}$. At some point in time, the almost synchronized motion is then again interrupted by a brief outburst of only partial synchronization. This finding is in some analogy to the state-dependent vulnerability of synchronization reported in Ref. 50. It depends on both the state of the driven dynamics and the momentary input received from the driver, whether or not the almost fully synchronized motion breaks down temporarily. The mean duration of the almost synchronized dynamics vs the one of only partially synchronized motions is influenced by $\Delta\alpha$ and ε. Furthermore, these parameters determine whether generalized synchronization between the driver and response occurs [Figs. 5(c) and 5(d)] or not [Fig. 5(e)]. This further supports that the synchronization measures, in this case G, are essential to discriminate between different states, which seem very similar under visual inspection [Fig. 5(d) vs Fig. 5(e)]. Taken together, Figs. 5(b)–5(e) show that weak inter-layer couplings can destabilize the chimera state in the response layer, even if the driver layer is in a chimera state.

As indicated by cold colors on the right of Fig. 4(a), we get non-identical group alignment synchronization throughout the entire range of $\Delta\alpha$ for high enough inter-layer couplings. The line of synchronization onset is tilted from lower ε for negative $\Delta\alpha$ to higher ε for positive $\Delta\alpha$ [Fig. 4(h)]. The degree of group alignment synchronization becomes higher upon a further increase of ε, in particular, for smaller absolute values of $\Delta\alpha$ [Fig. 4(a)]. For $\Delta\alpha = 0$, magenta indicates that we get identical group alignment synchronization for $\varepsilon \geq 0.215$. Looking at the underlying dynamics, we see that the phase velocity profile of the response is, in fact, identical to the one of the driver: $\omega_{x,j}(t) = \omega_{y,j}(t)$ [Fig. 5(a) vs Figs. 5(f) and 5(h)]. Recall, however, that even at $\Delta\alpha = 0$, the driver and the response layer are not identical since we use a non-zero $\Delta\nu$. Accordingly, the two layers of our network cannot synchronize identically. This aspect can only be resolved with the help of further synchronization metrics in the following.

The global pattern of the accumulated order parameter phase difference S in Fig. 4(c) resembles the pattern of $\overline{\Delta C}$ in Fig. 4(a). For uncoupled layers, the measure increases from $S = 2679$ at $\Delta\alpha = -0.036$ to $S = 3046$ at $\Delta\alpha = 0.036$. This can be explained by the influence of α_y on the average angular frequency of $Z_y(t)$, while the one of $Z_x(t)$ remains unaffected. A dark tongue in the S profile is found around the same area as in the $\overline{\Delta C}$ profile. These results reaching $S > 3700$ show that around these parameter values, the driving not only destabilizes the chimera state [see again Fig. 5(b)] but also reduces the average angular velocity of the response mean-field $Z_y(t)$. As a consequence of this deceleration, the order parameter of Y is lapped more often by the one of X, explaining the increase in S. In continued resemblances to the $\overline{\Delta C}$ profile, we find a white tongue of small S values within the unsynchronized regime of the left of Fig. 4(a). However, S generally remains above one. Accordingly, in this region of the $\Delta\alpha$–ε plane, the order parameter phase difference $\Delta\Phi(t)$ shows a stick-jump behavior. The sticking periods coincide with the almost fully synchronized states, whereas the outbursts of partial synchronization cause jumps [Figs. 5(c)–5(e)], resulting in low S values without reaching weak phase-locking. The exception is found at $\varepsilon = 0.04$ and $\Delta\alpha - 0.034$, where the sticking periods are typically longer than the evaluation interval. In consequence, at this isolated parameter value pair, we get $S < 1$ and, therefore, order parameter phase synchronization with weak phase-locking [see the isolated blue dot on the lower-left part of Fig. 4(c)].

Comparing again Figs. 4(a) and 4(c), or alternatively regarding Fig. 4(h), we find that for positive $\Delta\alpha$, the order parameter phase synchronization with weak phase-locking starts at somewhat higher ε than group alignment synchronization. For negative $\Delta\alpha$, both types of synchronization start within a more narrow range of ε. Within the phase synchronized regime, decreasing S values, indicating diminishing fluctuations in the order parameter phase difference $\Delta\Phi(t)$, are found for decreasing absolute $\Delta\alpha$ values [Fig. 4(c)]. For $\Delta\alpha = 0$ and $\varepsilon \geq 0.215$, magenta indicates that the fluctuations disappear and we get $S = 0$. Hence, we detect order parameter phase synchronization with strong phase-locking. This is plausible since we saw above that the phase velocity profiles $\omega_{x,j}(t)$ and $\omega_{y,j}(t)$ are identical for $\Delta\alpha = 0$ and $\varepsilon \geq 0.215$ [see again Fig. 5(a) vs Fig. 5(f) and see Fig. 5(h)].

Turning to the measure K, which assesses the order parameter amplitude correlation, we find that also here, results for $\Delta\alpha = 0$ and $\varepsilon \geq 0.215$ stands out [magenta in Fig. 4(d)]. We get an order parameter amplitude correlation of $K = 1$, implying that the

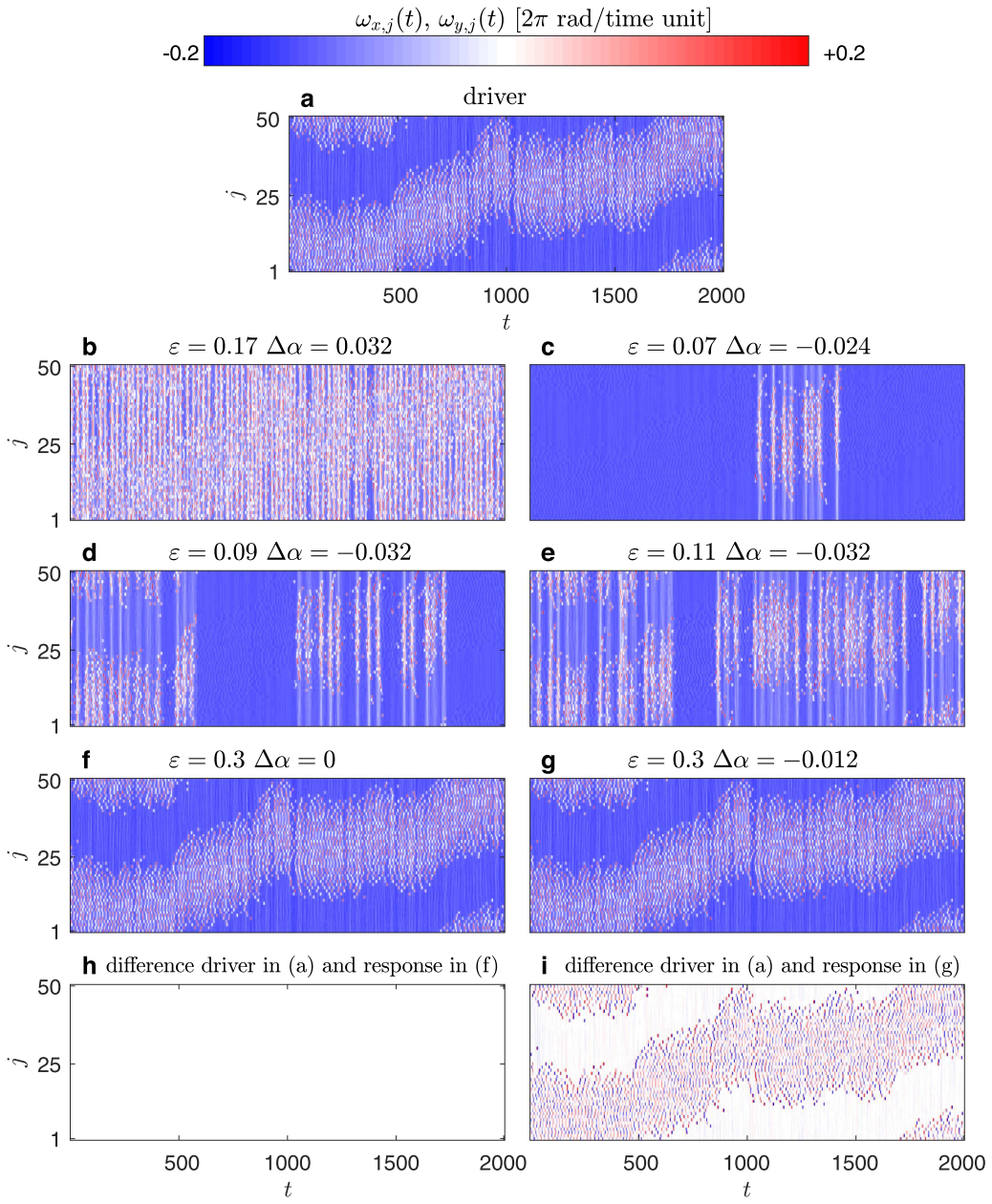

FIG. 5. The driver chimera can destabilize the response chimera. (a) Profiles of instantaneous frequencies $\omega_{x,j}(t)$ for the driver X (the same realization and the time window as in Fig. 1). (b)–(g) The same as (a) but for the response: $\omega_{y,j}(t)$. Inter-layer coupling ε and mismatch in phase lag parameter $\Delta\alpha$ indicated above each panel. Other parameters: $N = 50$, $b = 18$, $\nu_x = 0$, $\nu_y = 0.2$ (i.e., $\Delta\nu = 0.2$). (h) $\omega_{x,j}(t) - \omega_{y,j}(t) = 0$ for the example of $\varepsilon = 0.3$ and $\Delta\alpha = 0$. (i) $\omega_{x,j}(t) - \omega_{y,j}(t) \neq 0$ for the example of $\varepsilon = 0.3$ and $\Delta\alpha = -0.012$. The color scale in panels (h) and (i) is the same as in (a)–(g) but bounded by -0.02 and $+0.02$. All panels have the same range of j and t.

temporal variations of these amplitudes are identical for the driver and response. Moreover, there is no constant offset between $R_x(t)$ and $R_y(t)$ (results not shown). Hence, we get identical order parameter amplitude synchronization between X and Y. Also, these K results are consistent with, but not sufficient for, identical synchronization between the driver and response at zero mismatch in α and strong enough inter-layer coupling ε. Recall again that we can rule out identical synchronization *a priori* since the two layers are non-identical. For zero inter-layer coupling, $K \approx 0$ is found, and only small K values are obtained for weak coupling.

Remarkably, the onset of order parameter phase synchronization with weak phase-locking is accompanied by a first sharp increase of order parameter amplitude correlation K [see Fig. 4(c) vs Fig. 4(d)]. Upon a further increase of ε, the threshold of $K \geq 0.99$ for non-identical order parameter amplitude synchronization is reached, resulting in a triangular pattern with its tip at the point $\Delta\alpha = 0$ and $\varepsilon = 0.215$.

Combining the results for the order parameter phases [Fig. 4(c)] and order parameter amplitudes [Fig. 4(d)], we see a transition from (i) an unsynchronized motion, to (ii) phase synchronization with weak phase-locking but without amplitude synchronization, to (iii) phase synchronization with weak phase-locking and non-identical amplitude synchronization, and reaching (iv) phase synchronization with strong phase-locking and identical amplitude synchronization. Evidently, the exact value of ε leading to the transition from (ii) to (iii) depends on the choice of the threshold $K \geq 0.99$ used for the detection of non-identical amplitude synchronization.

We illustrated above that at $\Delta\alpha = 0.028$ and upon increasing ε at first, the order parameters and only later individual oscillator pairs show weak phase-locking (see again Table I, columns S and L_w and Fig. 3). It turns out that this cascaded synchronization onset is found throughout positive $\Delta\alpha$. For negative $\Delta\alpha$, the onset of partial weak phase-locking of individual oscillator pairs practically coincides with the one of weak phase-locking between the order parameters [compare again Fig. 4(c) vs Fig. 4(e) and see Fig. 4(h)]. Like for all previous synchronization measures, the line $\Delta\alpha = 0$ and $\varepsilon \geq 0.215$ stands out [magenta in Fig. 4(e)]. Here, and only here, we find complete oscillator pair phase synchronization with strong phase-locking, reflected in $L_s = 1$. This is confirmed by comparing Fig. 5(a) vs Fig. 5(f) and by Fig. 5(h), which shows $\omega_{y,j}(t) = \omega_{x,j}(t)$ obtained for exemplary parameters on the magenta line. Away from the magenta line, we always get $L_s = 0$, indicating the absence of strong phase-locking between individual oscillator pairs. This is confirmed by comparing Fig. 5(a) vs Fig. 5(g) and by Fig. 5(i), which show non-zero differences between $\omega_{y,j}(t)$ and $\omega_{x,j}(t)$ obtained for exemplary parameters away from the magenta line. In consequence, we either get $L_s = 0$ or $L_s = 1$. We never find partial oscillator pair phase synchronization with strong phase-locking, which would be reflected in $0 < L_s < 1$.

A look at the average phase differences for the order parameters [Fig. 4(f)] and for pairs of individual oscillators (not shown) allows resolving the particular type of synchronization found for $\Delta\alpha = 0$ and $\varepsilon \geq 0.215$. Recall that these average phase differences are only meaningfully defined for parameter values at which we get phase-locking. For the order parameters, we find $\overline{\Delta\Phi} < 0$, implying that expectedly, the response Y lags behind the driver X [Fig. 4(f)]. With increasing inter-layer coupling ε, the absolute value of this lag decreases throughout the range of $\Delta\alpha$. In contrast to all synchronization measures discussed above, however, the line $\Delta\alpha = 0$ and $\varepsilon \geq 0.215$ does not stand out in the $\overline{\Delta\Phi}$ profile. On the other hand, inspecting the phase differences between individual oscillator pairs $\overline{\Delta\phi_j}$, one finds that exclusively for parameters on this line, the phase lag is constant not only across time but also across all oscillators (results not shown). In consequence, the order parameters rotate with the same time-independent phase lag between them: $\Delta\Phi(t) = \Delta\phi_j(t) = \Delta\Phi_0$ for all j, which is also confirmed by $S = 0$. Basically, at any moment in time, the response is a replica of the drive with all oscillators rotated by a constant angle $\Delta\Phi_0$. This rotation has no effect on the order parameter lengths such that $K = 1$. It also does not alter the instantaneous frequencies, explaining why we get $\omega_{y,j}(t) = \omega_{x,j}(t)$ across all t and j. The latter equality in turn explains the identical group alignment synchronization found for $\Delta\alpha = 0$ and $\varepsilon \geq 0.215$, because the average chimera group distance $\overline{\Delta C}$ is based on $\omega_{y,j}(t)$ and $\omega_{x,j}(t)$. Effectively, at $\Delta\alpha = 0$, all individual oscillator pairs and, therefore, the two layers of the network behave like a pair of simple coupled oscillators with a mismatch in their natural frequencies. Above a certain coupling strength, they enter into synchronization with a non-zero but constant phase lag. This analogy is plausible when we recall again that at $\Delta\alpha = 0$, only the mismatch $\Delta\nu = 0.2$ between the frequencies of the driver and response remains.

We close this section by describing the onset of generalized synchronization with regard to the other types of synchronization [Fig. 4(g)]. We have shown above (Fig. 1 and Table I) that at $\Delta\alpha = 0.028$ and upon increasing ε, we get the following sequence of onsets: non-identical group alignment synchronization ($0 < \overline{\Delta C} \leq 0.05$), order parameter phase synchronization with weak phase-locking ($0 < S < 1$), generalized synchronization ($G = 1$), partial oscillator pair phase synchronization with weak phase-locking ($1 > L_w \geq 0.5$), and finally non-identical order parameter amplitude synchronization ($1 > K \geq 0.99$). This cascaded synchronization onset is found across $\Delta\alpha > 0$ [compare again Figs. 4(a), 4(c), 4(d), 4(e), and 4(g) and see Fig. 4(h)]. For $\Delta\alpha = 0$, all types of synchronization have their onset at $\varepsilon = 0.215$, directly entering into their strongest degree. For $\Delta\alpha < 0$, except for non-identical order parameter amplitude synchronization, all synchronization types have their onset within a narrow range of ε [Fig. 4(h)]. Concerning the critical couplings, one should again keep in mind that their exact values depend on the exact choice of the different thresholds used for the definition of the synchronization onsets (see also Refs. 8, 11, and 31). With regard to generalized synchronization vs phase synchronization,[51] we see that we can get order parameter phase synchronization without generalized synchronization at $\Delta\alpha > 0$, as well as order parameter phase synchronization along with generalized synchronization $\Delta\alpha \leq 0$. Can we get generalized synchronization without phase synchronization? Yes, this is given in the tongue centered around inter-layer couplings of $\varepsilon = 0.05$ for negative $\Delta\alpha$ [Fig. 4(h)].

V. DISCUSSION

The network studied here provides an example of a modular system in which the coupling within and across modules is established via connections between individual nodes. Depending on its parameters, the system can show different forms and degrees of partial synchronization. Furthermore, part of the network can transiently or permanently collapse to an almost fully synchronized motion. These features of the network structure and dynamics can be regarded as analogies to the brain, its functions and diseases, leading to potential applicability of our findings to real-world dynamics (see also Refs. 12, 17, 19, 20, 22, 36, 45, and 52–60). However, our network is far away from being a realistic model for the brain. It is much too simple. It might, however, be exactly this simplicity that yields our network a powerful model. It allows us to study basic

mechanisms of synchronization, which the brain may also employ to orchestrate its functions. The brain is complex, but it might still make use of simple principles.

Depending only on its parameter $\Delta\alpha$, our network can show different transitions to synchronization between the driver X and response Y. For example, for negative $\Delta\alpha$, it shows a sharp transition where most types of synchronization start in a narrow range of inter-layer coupling. Beyond this coupling, the drifting motion of the low-coherence group in the response is very similar to the one in the driver, and all individual oscillators as well as the mean-field are phase-locked. Moreover, the driver and response show generalized synchronization.[6] Here, we should recall the implication of generalized synchronization. The state of the response has become independent from its initial condition and depends solely on the state of the driver. Furthermore, at this transition, the mean-field amplitudes show a strong increase in the across-layer correlation, however, without reaching the threshold for order parameter amplitude synchronization. In contrast, for the non-multiplex setting studied in Ref. 20, the mean-field amplitudes remained uncorrelated across the two layers despite locking of the mean-field phases.

For positive $\Delta\alpha$, our system shows a more cascaded onset of synchronization. Shepelev and Vadivasova also reported on such a cascaded onset, in their case frequency synchronization and structure synchronization started at different inter-layer coupling strengths.[8] One exemplary stage of the cascade we find here are intermediate coupling strengths at which the phases of the mean-fields are already locked with only a moderate correlation between the mean-field amplitudes. At the same coupling, all individual oscillators remain unsynchronized across layers. Furthermore, there is no generalized synchronization, which implies that the response layer, despite being mean-field phase-locked to the driver, still carries the information of its initial conditions. Small changes of the coupling strength can be used to up- or down-regulate the mean-field amplitude correlation without affecting the other synchronization quantities. Upon an increase of the coupling, an adjustable fraction of individual nodes can be pushed into a phase-locked motion, which is in analogy to previous findings.[21,30,32] Overall, the system has the capacity to achieve tunable degrees of across-layer synchronization of macroscopic mean-field variables, while microscopic variables can remain unsynchronized. It is also capable of allowing the driver to entrain the response with regard to both microscopic and macroscopic variables and force the response to forget its initial conditions via generalized synchronization. Last but not least, forcing the response to forget its initial conditions can also be achieved without entrainment of the mean-fields. The chimeric balance between synchronization and de-synchronization within individual layers can furthermore co-exist with the different across-layer synchronization types. The across-layer driving can, however, also push the response layer into a state of almost full within-layer synchronization or desynchronization. In this case, any type of across-layer synchronization might only be an epiphenomenon of the response dynamics' degeneration. It can be conjectured that this collapse corresponds to some malfunction of the system. The existence of such malfunctions could be the price the system has to pay for its versatility of functions.

In closing, we briefly sketch some open questions. The phase lag parameter is important for the emergence of chimera states (see, for example, Refs. 1, 3, 52, 60, and 61). Along with the difference in the natural frequencies $\Delta\nu = \nu_y - \nu_x$, we used the difference of the phase lag parameters $\Delta\alpha = \alpha_y - \alpha_x$ to introduce a mismatch between the parameters of the driver and the response layer. Future work should study in more detail the role of the phase lag parameter in individual layers with regard to the emergence of chimera states in multilayer networks. Furthermore, the transient nature of chimera states[44,45,61,62] should be further analyzed. A question that should be addressed is how the inter-layer coupling influences the system's overall stability and lifetime distributions (see also Refs. 63 and 64). For example, does coupling between layers promote or prevent chimera state collapses to fully synchronized states within individual layers?

ACKNOWLEDGMENTS

We acknowledge funding from the Spanish Ministry of Science and Innovation and the State Research Agency (Grant No. PID2020-118196GBI00/MICIN/AEI/10.13039/501100011033).

AUTHOR DECLARATIONS

Conflict of Interest

The authors have no conflicts to disclose.

Author Contributions

Ralph G. Andrzejak: Conceptualization (lead); Formal analysis (lead); Investigation (lead); Methodology (lead); Resources (equal); Supervision (lead); Validation (equal); Visualization (equal); Writing – original draft (lead); Writing – review & editing (equal). **Anaïs Espinoso:** Formal analysis (supporting); Investigation (supporting); Resources (equal); Validation (equal); Visualization (equal); Writing – review & editing (equal).

DATA AVAILABILITY

The data that support the findings of this study are openly available in the electronic library repository of the Universitat Pompeu Fabra at https://dataverse.csuc.cat/dataverse/cat?q=andrzejak, Ref. 65.

REFERENCES

[1] Y. Kuramoto and D. Battogtokh, "Coexistence of coherence and incoherence in nonlocally coupled phase oscillators," Nonlinear Phenom. Complex Syst. **5**, 380–385 (2002).
[2] E. Montbrió, J. Kurths, and B. Blasius, "Synchronization of two interacting populations of oscillators," Phys. Rev. E **70**, 056125 (2004). DOI:
[3] D. M. Abrams and S. H. Strogatz, "Chimera states for coupled oscillators," Phys. Rev. Lett. **93**, 174102 (2004).
[4] Y. Maistrenko, S. Brezetsky, P. Jaros, R. Levchenko, and T. Kapitaniak, "Smallest chimera states," Phys. Rev. E **95**, 010203 (2017).
[5] R. G. Andrzejak, "Chimeras confined by fractal boundaries in the complex plane," Chaos **31**, 053104 (2021).
[6] R. G. Andrzejak, G. Ruzzene, and I. Malvestio, "Generalized synchronization between chimera states," Chaos **27**, 053114 (2017).
[7] A. Bukh, E. Rybalova, N. Semenova, G. Strelkova, and V. Anishchenko, "New type of chimera and mutual synchronization of spatiotemporal structures in two coupled ensembles of nonlocally interacting chaotic maps," Chaos **27**, 111102 (2017).

[8]I. Shepelev and T. Vadivasova, "Synchronization in multiplex networks of chaotic oscillators with frequency mismatch," Chaos, Solitons Fractals **147**, 110882 (2021).
[9]I. Korneev, V. Semenov, A. Slepnev, and T. Vadivasova, "Complete synchronization of chaos in systems with nonlinear inertial coupling," Chaos, Solitons Fractals **142**, 110459 (2021).
[10]E. Rybalova, T. Vadivasova, G. Strelkova, and A. Zakharova, "Multiplexing noise induces synchronization in multilayer networks," Chaos, Solitons Fractals **163**, 112521 (2022).
[11]E. Rybalova, G. Strelkova, E. Schöll, and V. Anishchenko, "Relay and complete synchronization in heterogeneous multiplex networks of chaotic maps," Chaos **30**, 061104 (2020).
[12]J. Sawicki, I. Omelchenko, A. Zakharova, and E. Schöll, "Delay controls chimera relay synchronization in multiplex networks," Phys. Rev. E **98**, 062224 (2018).
[13]M. Winkler, J. Sawicki, I. Omelchenko, A. Zakharova, V. Anishchenko, and E. Schöll, "Relay synchronization in multiplex networks of discrete maps," Europhys. Lett. **126**, 50004 (2019).
[14]E. Rybalova, T. Vadivasova, G. Strelkova, V. Anishchenko, and A. Zakharova, "Forced synchronization of a multilayer heterogeneous network of chaotic maps in the chimera state mode," Chaos **29**, 033134 (2019).
[15]G. I. Strelkova, T. E. Vadivasova, and V. S. Anishchenko, "Synchronization of chimera states in a network of many unidirectionally coupled layers of discrete maps," Regul. Chaotic Dyn. **23**, 948–960 (2018).
[16]I. Omelchenko, T. Hülser, A. Zakharova, and E. Schöll, "Control of chimera states in multilayer networks," Front. Appl. Math. Stat. **4**, 67 (2018).
[17]M. Mikhaylenko, L. Ramlow, S. Jalan, and A. Zakharova, "Weak multiplexing in neural networks: Switching between chimera and solitary states," Chaos **29**, 023122 (2019).
[18]G. Ruzzene, I. Omelchenko, J. Sawicki, A. Zakharova, E. Schöll, and R. G. Andrzejak, "Remote pacemaker control of chimera states in multilayer networks of neurons," Phys. Rev. E **102**, 052216 (2020).
[19]K. Anesiadis and A. Provata, "Synchronization in multiplex leaky integrate-and-fire networks with nonlocal interactions," Front. Netw. Physiol. **2**, 910862 (2022).
[20]R. G. Andrzejak, G. Ruzzene, I. Malvestio, K. Schindler, E. Schöll, and A. Zakharova, "Mean field phase synchronization between chimera states," Chaos **28**, 091101 (2018).
[21]D. Kasatkin and V. Nekorkin, "Synchronization of chimera states in a multiplex system of phase oscillators with adaptive couplings," Chaos **28**, 093115 (2018).
[22]H. Sakaguchi, "Instability of synchronized motion in nonlocally coupled neural oscillators," Phys. Rev. E **73**, 031907 (2006).
[23]V. A. Maksimenko, V. V. Makarov, B. K. Bera, D. Ghosh, S. K. Dana, M. V. Goremyko, N. S. Frolov, A. A. Koronovskii, and A. E. Hramov, "Excitation and suppression of chimera states by multiplexing," Phys. Rev. E **94**, 052205 (2016).
[24]S. Ghosh, A. Kumar, A. Zakharova, and S. Jalan, "Birth and death of chimera: Interplay of delay and multiplexing," Europhys. Lett. **115**, 60005 (2016).
[25]S. Majhi, M. Perc, and D. Ghosh, "Chimera states in a multilayer network of coupled and uncoupled neurons," Chaos **27**, 073109 (2017).
[26]A. Dmitrichev, D. S. Shchapin, and V. I. Nekorkin, "Cloning of chimera states in a multiplex network of two-frequency oscillators with linear local couplings," JETP Lett. **108**, 543–547 (2018).
[27]T. Vadivasova, A. Slepnev, and A. Zakharova, "Control of inter-layer synchronization by multiplexing noise," Chaos **30**, 091101 (2020).
[28]E. Rybalova, G. Strelkova, and V. Anishchenko, "Impact of sparse inter-layer coupling on the dynamics of a heterogeneous multilayer network of chaotic maps," Chaos, Solitons Fractals **142**, 110477 (2021).
[29]M. Chen, D. Veeman, Z. Wang, and A. Karthikeyan, "Chimera states in a network of identical oscillators with symmetric coexisting attractors," Eur. Phys. J. Spec. Top. **231**(11), 2163–2171 (2022).
[30]I. A. Shepelev, A. Bukh, T. E. Vadivasova, and V. S. Anishchenko, "Synchronization effects for dissipative and inertial coupling between multiplex lattices," Commun. Nonlinear Sci. Numer. Simul. **93**, 105489 (2021).
[31]I. Shepelev, A. Bukh, G. Strelkova, and V. Anishchenko, "Anti-phase relay synchronization of wave structures in a heterogeneous multiplex network of 2D lattices," Chaos, Solitons Fractals **143**, 110545 (2021).
[32]A. V. Bukh, E. Schöll, and V. Anishchenko, "Synchronization of spiral wave patterns in two-layer 2D lattices of nonlocally coupled discrete oscillators," Chaos **29**, 053105 (2019).
[33]D. Kasatkin, S. Yanchuk, E. Schöll, and V. Nekorkin, "Self-organized emergence of multilayer structure and chimera states in dynamical networks with adaptive couplings," Phys. Rev. E **96**, 062211 (2017).
[34]Z.-M. Wu, H.-Y. Cheng, Y. Feng, H.-H. Li, Q.-L. Dai, and J.-Z. Yang, "Chimera states in bipartite networks of FitzHugh–Nagumo oscillators," Front. Phys. **13**, 130503 (2018).
[35]Q. Dai, Q. Liu, H. Cheng, H. Li, and J. Yang, "Chimera states in a bipartite network of phase oscillators," Nonlinear Dyn. **92**, 741–749 (2018).
[36]A. Rontogiannis and A. Provata, "Chimera states in FitzHugh–Nagumo networks with reflecting connectivity," Eur. Phys. J. B **94**, 97 (2021).
[37]N. F. Rulkov, M. M. Sushchik, L. S. Tsimring, and H. D. I. Abarbanel, "Generalized synchronization of chaos in directionally coupled chaotic systems," Phys. Rev. E **51**, 980–994 (1995).
[38]H. D. I. Abarbanel, N. F. Rulkov, and M. M. Sushchik, "Generalized synchronization of chaos: The auxiliary system approach," Phys. Rev. E **53**, 4528 (1996).
[39]L. Kocarev and U. Parlitz, "Generalized synchronization, predictability, and equivalence of unidirectionally coupled dynamical systems," Phys. Rev. Lett. **76**, 1816 (1996).
[40]M. G. Rosenblum, A. S. Pikovsky, and J. Kurths, "Phase synchronization of chaotic oscillators," Phys. Rev. Lett. **76**, 1804–1807 (1996).
[41]Y. Kuramoto, *Chemical Oscillations, Waves, and Turbulence* (Springer, 1984).
[42]O. E. Omel'chenko, M. Wolfrum, and Y. L. Maistrenko, "Chimera states as chaotic spatiotemporal patterns," Phys. Rev. E **81**, 065201 (2010).
[43]S. R. Jammalamadaka and A. Sengupta, *Topics in Circular Statistics* (World Scientific, 2001), Vol. 5.
[44]M. Wolfrum and O. E. Omel'chenko, "Chimera states are chaotic transients," Phys. Rev. E **84**, 015201 (2011).
[45]R. G. Andrzejak, C. Rummel, F. Mormann, and K. Schindler, "All together now: Analogies between chimera state collapses and epileptic seizures," Sci. Rep. **6**, 23000 (2016).
[46]Like argued in Ref. 6, $\delta(t)$ is best suited to numerically test for generalized synchronization. By Eq. (17) phase differences ranging from 0 to 2π are mapped to one sinus half wave, assigning the maximal difference of one to a phase difference of π. Without the division by two, phase differences of (close to) π would count as (close to) zero. As an alternative, one might use the order parameter of phase differences $\frac{1}{N}|\sum_j e^{i(\phi_{x,j}(t)-\phi_{y,j}(t))}|$. However, due to its low absolute slope at small arguments, this order parameter is numerically indistinguishable from one for phase difference orders of magnitude higher than the limit of the numerical precision. In contrast, having an absolute slope of one at small arguments, Eq. (17) remains sensitive to phase differences down to this limit. Following Ref. 47, any value $\delta(t) < 10^{-13}$ is assumed to be zero. This is because the underlying sine function has values of up to the order of 10^0. Accordingly, values on the order of 10^{-14}–10^{-16} are just above the resolution of the double floating point precision.[48] We, therefore, assume that such nonzero but very small values arise from the limited floating point precision and report them to be zero.
[47]R. G. Andrzejak, G. Ruzzene, E. Schöll, and I. Omelchenko, "Two populations of coupled quadratic maps exhibit a plentitude of symmetric and symmetry broken dynamics," Chaos **30**, 033125 (2020).
[48]IEEE Standards Committee, "IEEE standard for floating-point arithmetic," in *IEEE Std 754-2008* (IEEE Computer Society, 2008), pp. 1–70.
[49]Regarding the well-known bump-shaped average phase velocity profile displayed in Fig. 3(c) of Ref. 1, one has to keep in mind that phase velocities are negative to realize that oscillators in the high-coherence group rotate faster than the ones in the low-coherence group. Oscillators in the high-coherence group often lap the ones in the low-coherence group.
[50]E. S. Medeiros, R. O. Medrano-T, I. L. Caldas, T. Tél, and U. Feudel, "State-dependent vulnerability of synchronization," Phys. Rev. E **100**, 052201 (2019).
[51]Z. Zheng and G. Hu, "Generalized synchronization versus phase synchronization," Phys. Rev. E **62**, 7882–7885 (2000).
[52]D. Abrams, R. Mirollo, S. Strogatz, and D. Wiley, "Solvable model for chimera states of coupled oscillators," Phys. Rev. Lett. **101**, 084103 (2008).

[53]A. Rothkegel and K. Lehnertz, "Irregular macroscopic dynamics due to chimera states in small-world networks of pulse-coupled oscillators," New J. Phys. **16**, 055006 (2014).
[54]J. Hizanidis, N. E. Kouvaris, Z.-L. Gorka, A. Díaz-Guilera, and C. G. Antonopoulos, "Chimera-like states in modular neural networks," Sci. Rep. **6**, 19845 (2016).
[55]T. Chouzouris, I. Omelchenko, A. Zakharova, J. Hlinka, P. Jiruska, and E. Schöll, "Chimera states in brain networks: Empirical neural vs modular fractal connectivity," Chaos **28**, 045112 (2018).
[56]K. Bansal, J. O. Garcia, S. H. Tompson, T. Verstynen, J. M. Vettel, and S. F. Muldoon, "Cognitive chimera states in human brain networks," Sci. Adv. **5**, eaau8535 (2019).
[57]M. Gerster, R. Berner, J. Sawicki, A. Zakharova, A. Skoch, J. Hlinka, K. Lehnertz, and E. Schöll, "FitzHugh–Nagumo oscillators on complex networks mimic epileptic-seizure-related synchronization phenomena," Chaos **30**, 123130 (2020).
[58]T. A. Glaze and S. Bahar, "Neural synchronization, chimera states and sleep asymmetry," Front. Netw. Physiol. **1**, 734332 (2021).
[59]M. Masoliver, J. Davidsen, and W. Nicola, "Embedded chimera states in recurrent neural networks," Commun. Phys. **5**, 205 (2022).
[60]R. C. Budzinski, T. T. Nguyen, J. Doàn, J. Mináč, T. J. Sejnowski, and L. E. Muller, "Geometry unites synchrony, chimeras, and waves in nonlinear oscillator networks," Chaos **32**, 031104 (2022).
[61]M. Shanahan, "Metastable chimera states in community-structured oscillator networks," Chaos **20**, 013108 (2010).
[62]T. Lilienkamp and U. Parlitz, "Susceptibility of transient chimera states," Phys. Rev. E **102**, 032219 (2020).
[63]J. L. Ocampo-Espindola, E. Omel'chenko, and I. Z. Kiss, "Non-monotonic transients to synchrony in Kuramoto networks and electrochemical oscillators," J. Phys.: Complex. **2**, 015010 (2021).
[64]E. Omel'chenko and T. Tél, "Focusing on transient chaos," J. Phys.: Complex. **3**, 010201 (2022).
[65]Open access library repository, Universitat Pompeu Fabra; see https://dataverse.csuc.cat/dataverse/cat?q=andrzejak.